Available online at www.sciencedirect.com
SCIENCE DIRECT
Journal of Solid State Chemistry 179 (2006) 1296–1302
JOURNAL OF SOLID STATE CHEMISTRY
www.elsevier.com/locate/jssc

A novel ferrimagnetic irido-cuprate: $IrSr_2GdCu_2O_8$

A.J. Dos Santos-García, Myriam H. Aguirre, E. Morán, R. Saez Puche, M.Á. Alario-Franco*

Laboratorio de Química del Estado Sólido, Departamento de Química Inorgánica, and Laboratorio Complutense de Altas presiones, Facultad de Química, Universidad Complutense, EU 28040 Madrid, Spain

Received 11 November 2005; received in revised form 19 December 2005; accepted 22 December 2005
Available online 13 March 2006

Abstract

We have performed an investigation of the structural, microstructural and magnetic properties of the new compound $IrSr_2GdCu_2O_8$. The sample was prepared under high temperature (~1393 K) and high-pressure conditions (~60 Kbars) in a Belt type apparatus. X-ray diffraction (XRD) analysis shows that this irido-cuprate is isostructural with the corresponding Ru-1212 phase. Structurally, this material shows an interesting hierarchy of ordering phenomena, whose observation actually depends on the technique used to analyze the material: from a "simple" cell $a_p \times a_p \times 3a_p$ which is supported by XRD, through a "diagonal" one, $\sim\sqrt{2}a_p \times \sqrt{2}a_p \times 3a_p$ as seen by SAED, to a microdomain texture of this last one cell supported by HREM. A ferrimagnetic Ir^{IV}–Gd^{III} spin ordering is observed below 15 K. The iridium oxidation state seems to be +4.

Keywords: Irido-cuprate; High pressure synthesis; Ferrimagnetism; Crystal structure; Microstructure

1. Introduction

There has recently been an important research activity in a series of materials loosely called "ruthenates" or "rutheno-cuprates" of general formula $RuSr_2RECu_2O_8$ [1–5] where RE is a rare-earth trivalent cation. These formally derive from the classical Ybco superconductor, $Ba_2YCu_3O_7$ which, taking into account its structural and physico-chemical characteristics, is best formulated [6,7] as $YCuBa_2Cu_2O_7$. These materials can be described by replacing the tetracoordinated square planar copper [Cu–O_4] in the "chains", forming the "charge reservoir layer", for octahedral [M–O_6] groups that form a perovskite-like layer in the basal plane of the unit cell. The earliest of these materials [8,9] which have M ⇌ Nb or Ta, where just semiconducting; however, the ruthenates have been shown to be both magnetic and superconducting [1,10,11] two properties that are usually consider antagonic [12] (see however Refs. [13,14]). Because of this, magnetic susceptibility of the ruthenates shows a peak at T_M~150 K followed, in decreasing the temperature, by a superconducting signature at ~30 K. This temperatures, in particular T_c, seem to depend very much of the synthesis conditions and it is not uncommon to obtain samples which are not superconducting. Under such circumstances, it is obviously not surprising that a number of studies have been dedicated to modify the composition of $RuSr_2GdCu_2O_8$ so as to improve these properties [15] (see Ref. [15] and references there in). At room pressure one can in fact only obtain the materials with Sm, Eu and Gd and most work has been performed in the last one. Yet we have recently shown (Ruiz Bustos et al. [15–17]) that at high pressures and temperatures, the majority of the rare-earth elements can be introduced in the structure [15–17,22–25]; even more, the Y-case, i.e. $RuSr_2YCu_2O_8$ appears to be the material showing the higher temperature of the family, T_c~51 K [16,25]. A number of partial substitutions of the Ru or Sr atoms have also been performed, and Sn [18] and Cu [19] in the place of ruthenium seem to be the more effective in increasing T_c. Recently Ru partial substitutions by Ir have been

*Corresponding author. Fax: +34 91 394 43 52.
E-mail addresses: rsp92@quim.ucm.es (R. Saez Puche), maaf@quim.ucm.es (M.Á. Alario-Franco).
URL: http://www.ucm.es/info/labcoap/index.html.

0022-4596/$ - see front matter © 2006 Elsevier Inc. All rights reserved.
doi:10.1016/j.jssc.2005.12.038

performed [20,21] and it appears that this supressess both the superconducting and the magnetic transitions as the Ir content is increased, above 20%.

The complete substitution in the Ru position, that is replacement, has however been less frequent. We have recently obtained a series of, non superconducting, phases of general formula $CrSr_2RECu_2O_8$ [15,22], where Cr appears to be in the Cr(IV) oxidation state.

We report in here the synthesis, structural and microstructural characterization and magnetic properties of a new $IrSr_2GdCu_2O_8$ compound that we have obtained at high pressure and temperature.

2. Experimental

Samples were prepared in a two-step process: a mixed Sr–Cu oxide of the appropriate stoichiometry was prepared according to

$$SrCO_3 + CuO \rightarrow SrCuO_2 + CO_2, \quad (1)$$

by heating at 1323 K in air for 3 days. Then, this precursor was thoroughly mixed with the appropriate amounts of Gd_2O_3 and IrO_2 oxides (AR, Sigma Aldrich) placed within a platinum capsule and treated in a Belt-type apparatus according to

$$2SrCuO_2 + \tfrac{1}{2}RE_2O_3 + IrO_2 + \tfrac{1}{4}O_2 \rightarrow IrSr_2RECu_2O_8, \quad (2)$$

where in analogy to the ruthenates and chromates, oxygen is taken from the atmosphere [15,22] within a grid of 60 ± 20 Kbar, 1400 ± 200 K and 60 ± 30 min; the best conditions to obtain the material are 60 Kbar, 1373 K and 90′.

The samples have been characterized by means of X-ray diffraction (XRD) powder diffraction performed in a Siemens D-500 diffractometer (Cu$K\alpha$ source, Ni filter).

The XRD patterns were refined with the Rietveld procedure using the fullprof program [26]. As a starting model we used the structure previously reported by Attfield et al. for $RuSr_2GdCu_2O_8$. Backgrounds were fitted using a linear interpolation and peak shapes were modelled by a pseudo-Voigt function.

The sample composition was checked by EDS (Link Pentafet 5947 Model, Oxford Microanalysis Group) in a Transmission Electron Microscopy (TEM) (Jeol JEM FX2000) by in situ observations.

High-resolution TEM and SAED were performed on a Jeol JEM 3000 EX microscope.

Magnetic susceptibility measurements were made at different magnetic field strengths over the temperature range 1.9–300 K, using a Squid Quantum Design XL-MPMS magnetometer in zero field cooling (ZFC) and field cooling (FC) conditions. The variation of the magnetization as a function of the magnetic field was measured in the field range from −5 to 5 T at 2.5, 7 and 12 K.

3. Results and discussion

The XRD of the sample, Fig. 1, did show the presence of a pattern that, by analogy with the rutheno-cuprates and chromo-cuprates, can be indexed as $IrSr_2GdCu_2O_8$.

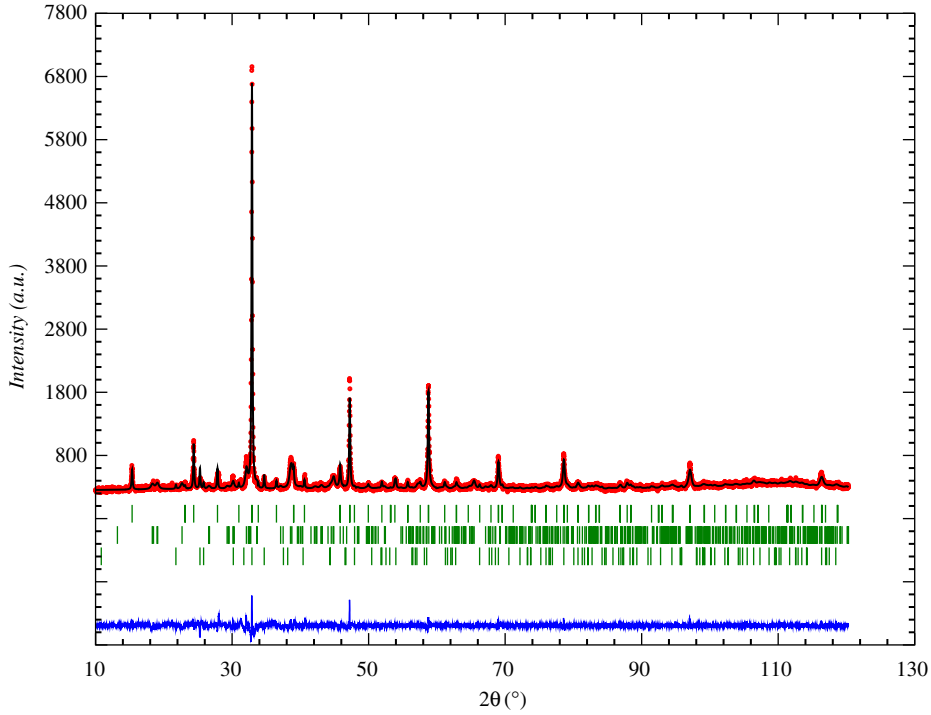

Fig. 1. Rietveld refinement fit of the X-ray diffraction data for (1) $IrSr_2GdCu_2O_8$. Sr_3IrCuO_6 (2) and $SrCuO_2$ (3) are present as impurities.

Table 1
Refined cell and atomic parameters and agreement factors for the $IrSr_2GdCu_2O_8$ with space group $P4/mmm$

T (K)	a (Å)	c (Å)	V (Å^3)	R_{wp}	R_p	χ^2
298	3.8460(1)	11.5301(7)	170.55(1)	0.0727	0.0548	1.84
Atom	Site	x	y	z	U_{iso} (Å^2)	Occupancy
Ir	1(b)	0	0	0.5	0.023(2)	1
Sr	2(h)	0.5	0.5	0.3094(4)	0.007(2)	1
Gd	1(c)	0.5	0.5	0	0.008(1)	1
Cu	2(g)	0	0	0.1466(6)	0.003(2)	1
O1	8(s)	0.07(2)	0	0.345(3)	0.025	0.25
O2	4(i)	0	0.5	0.139 (2)	0.025	1
O3	4(o)	0.130(9)	0.5	0.5	0.025	0.5

As often observed in H.P. samples of multi-cationic materials, some minor impurities, below 10%, appearing were identified as Sr_3IrCuO_6 (~6%) and $SrCuO_2$ (~3%). These were taken into account in both the refinement and magnetic properties [27–29]. A couple of very low intensity reflections could not be accounted for.

The metallic compositions of the three materials were confirmed by EDS in the electron microscope.

3.1. Crystal structure

The Rietveld refinement of the XRD data, Fig. 1; indicates that the *average* crystal structure of $IrSr_2GdCu_2O_8$ is tetragonal, space group $P4/mmm$, with parameters $a = 3.8460(1)$ Å, $c = 11.5301(2)$ Å, $c/a = 3.013$ and $V = 170.55$ Å^3. This new material is then isostructural with the corresponding Ru-1212 phase [15], whose parameters are $a = 3.8276(3)$ Å, $c = 11.5364(3)$ Å, $c/a = 3.014$ and $V = 168.017(1)$ Å^3. These values are on line with the bigger size of Ir^{IV}($^{VI}r_{Ir(IV)} = 0.625$ Å) than that of Ir^{V}($^{VI}r_{Ir(V)} = 0.57$ Å) to the average radius of Ru in $RuSr_2GdCu_2O_8$, where it has been shown [30] that there is a 60% Ru^{V} and 40% Ru^{IV} ratio, giving an average ratio of $^{VI}r_{Ru}^{4.6+} = 0.58$ Å.

Table 1 gives the refined cell and atomic parameters as well as the fit agreement factors for $IrSr_2GdCu_2O_8$. In the course of the refinement, we did take into account the usual splitting of the O(1) and O(3) positions observed in this structure [31]; the atomic thermal displacements, U_{iso}, corresponding to all oxygen ions, were fixed. Fig. 2 shows the crystal structure where the splitted positions of the above mentioned oxygen ions are apparent. On the other hand, Table 2 gives the interatomic distances and angles for this new Ir-1212 compound.

Neutron diffraction would be needed to fully establish the oxygen content; yet, all the 1212 materials obtained with ruthenium or chromium does not seem to show oxygen substoichiometry [5,22].

3.2. Magnetic properties

The susceptibility data shown in Fig. 3 follow a Curie–Weiss behaviour, $\chi = C/(T-\theta)$, in a wide range of temperatures, 15–300 K (see the inset on that figure) and the obtained magnetic moment takes the value of 8.14 μ_B with $\theta = -7.3$ K. For Ir^{V} ([Xe]$6s^2 4f^{14} 5d^4$), three types of electronic configurations are possible: in a weak octahedral field a high spin configuration $t_{2g}^3 e_g^1$ is expected; on the other hand, in a strong octahedral field such as in the present work a low spin configuration $t_{2g}^4 e_g^0$ takes place; on the other hand, in a strong tetragonal field an anisotropic electronic distribution ($d_{xz}^2 d_{yz}^2 d_{xy}^0 d_z^0 d_{x^2-y^2}^0$) can eventually be obtained [32]. Due to the large enhancement of the oxygen crystal field in the 5d series [33], the low spin configuration ($t_{2g}^4 e_g^0$) is to be expected.

The magnetic moment arising from this particular configuration is very much dependent on the spin–orbit coupling, giving as a result a characteristic temperature-independent paramagnetism arising from the non-degenerate ground term of Ir^{V}. Consequently Ir^{V} ions will not contribute to the cooperative magnetic interactions [34,35] and this could explain why no magnetic ordering has been observed in for example some double perovskites of the type Ba_2RIrO_6 [36], where the octahedral sites are randomly occupied by Ir^{V} and the rare-earth trivalent cation R^{III}.

Below 40 K, the observed—see inset on Fig. 3—downwards deviations from linearity in the reciprocal susceptibility can be attributed to incipient magnetic interactions. It is worth noting that at 15 K there is a shoulder in the susceptibility; this is indicative of an ordering transition, after which the χ still increases. This Curie–Weiss behaviour deviation could be explained assuming that not all Ir ions are pentavalent, and that, in analogy with the ruthenate there would be at the most a mixture of Ir^{V} and Ir^{IV} (see Refs. [11,30]).

However for the experimental moment of 8.14 μ_B, and considering that the gadolinium-free ion moment is 7.94 μ_B, the expected iridium moment is 1.79 μ_B which corresponds in fact to the theoretical Ir^{IV} moment [37].

If iridium is, indeed, tetravalent, for the composition $IrSr_2GdCu_2O_8$ it will be analogous to the case of Cr in $CrSr_2GdCu_2O_8$ [15,22], then, the copper oxidation state will be $Cu^{II}Cu^{III}$, with an average oxidation state of $Cu^{2.5+}$. This is away from the experimentally observed superconducting range for the cuprates

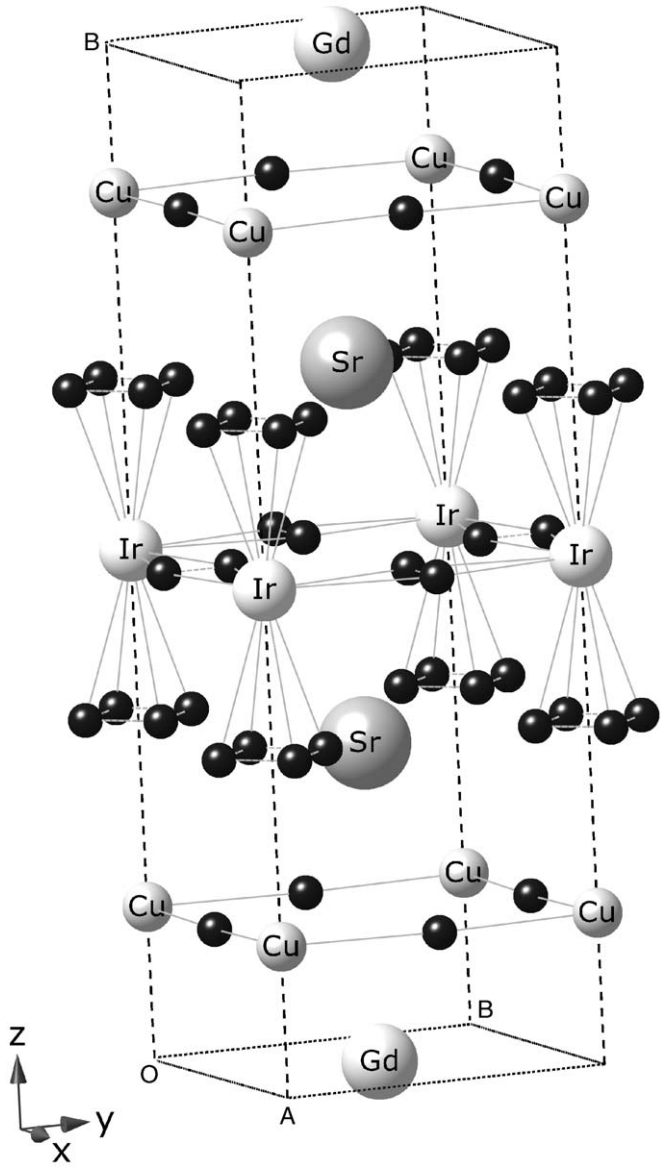

Fig. 2. Crystal structure of $IrSr_2GdCu_2O_8$: Note that the apical O(1) and equatorial O(2) ions are splitted into four and two positions, respectively.

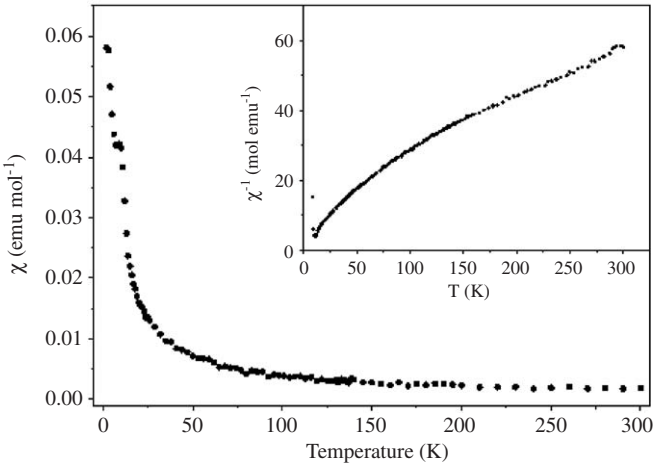

Fig. 3. Magnetic susceptibility (AC mode) as a function of temperature; notice the shoulder at ~15 K. In the inset the inverse of the magnetic susceptibility (DC mode) as a function of temperature is presented. It shows a Curie–Weiss behaviour.

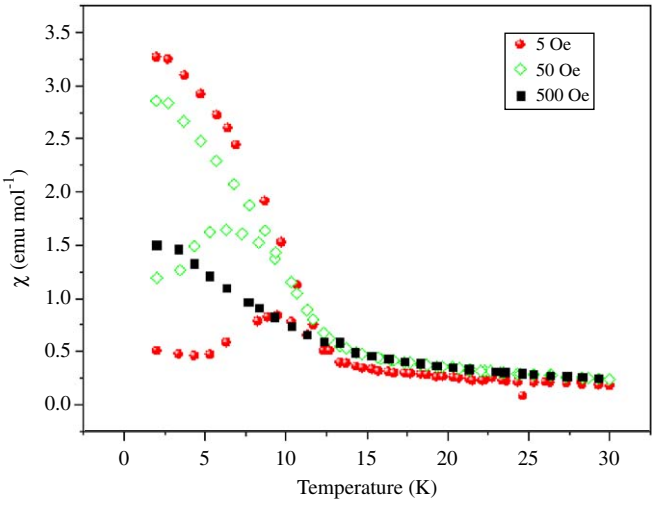

Fig. 4. FC and ZFC measurements of the magnetic susceptibility as a function of temperature. Irreversibility is clear.

Table 2
Some interatomic distances and angles in the $IrSr_2GdCu_2O_8$ structure

Distances (Å)		Angles (deg.)	
Cu–O(1) × 1	2.30(4)	O(1)–Cu–O(2)	91(2)
Cu–O(2) × 4	1.9250(9)	O(2)–Cu–O(2)	89.88(4)
Ir–O(1) × 2	1.81(3)	O(2)–Cu–O(2)	174.78(4)
Ir–O(3) × 4	1.987(9)	O(1)–Ir–O(1)	180
Gd–O(2) × 8	2.50(1)	O(1)–Ir–O(3)	82(2)
Sr–O(1) × 2	2.57(5)	O(3)–Ir–O(3)	90
Sr–O(1) × 2	2.94(5)	O(3)–Ir–O(3)	180
Sr–O(2) × 4	2.73(1)	Cu–O(1)–Ir	165.2(14)
Sr–O(3) × 2	2.618(4)	Cu–O(2)–Cu	174.78(4)
Sr–O(3) × 2	3.271(3)	Ir–O(3)–Ir	151(1)

(~2.05–2.25) [38]. In the case of $RuSr_2GdCu_2O_8$, an internal so-called self-doping mechanism $Ru^{V}_{1-x}Ru^{IV}_{x} \rightleftharpoons Cu^{II}_{1+x} + xCu^{III}_{x}$ is supposed to operate making an intermediate average oxidation state for copper that induces superconductivity [11]. This could explain why, unlike the ruthenium compounds and like the chromium ones, we do not observe superconductivity in this iridate. Even more, if a similar situation operates in the recently studied substitution of Ru by Ir in $Ru_{1-x}Ir_xSr_2GdCu_2O_8$ [20,21], that is if Ir enters as Ir^{IV}, it will increase the Cu^{III} concentration above the superconducting range and will suppress the superconductivity, as observed by Andrade et al. [20] and Torikachvili et al. [21].

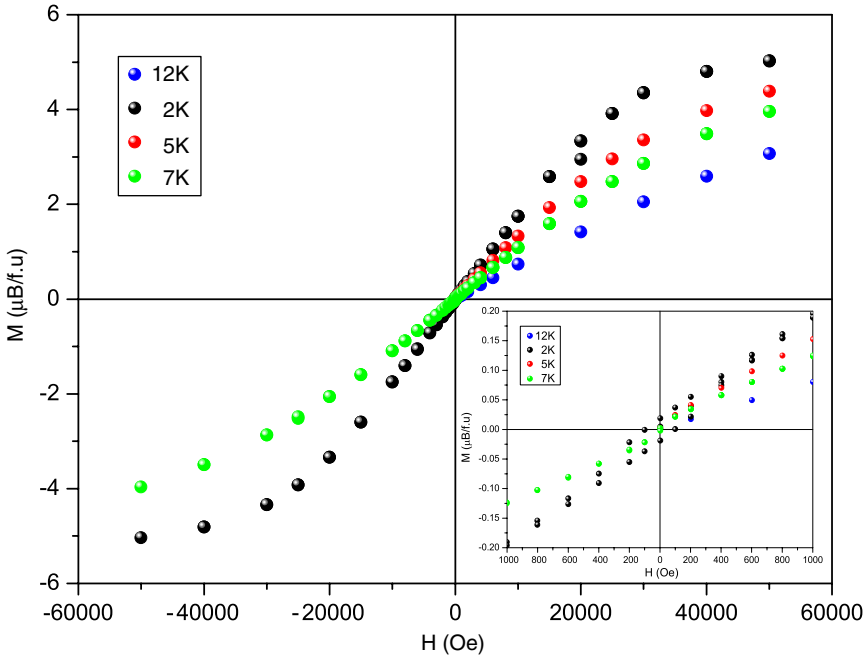

Fig. 5. The M vs. H curves at different temperatures below the transition point. Hysteresis appears at 2 K (see inset).

Below 15 K the susceptibility is field dependent, Fig. 4, and a marked irreversibility is observed when the FC and ZFC plots are compared. This phenomenon is characteristic of ferromagnetic interactions [39].

Hysteresis loops from -5 T to $+5$ T have been measured at different temperatures below the Curie one, see Fig. 5. A characteristic cycle for a ferromagnetic material is obtained at 2 K, with a remanence as low as 0.02 μ_B and a coercive field which takes the value of 100 Oe (see inset Fig. 5). This could be fully explained by considering the isotropic character associated to the $^8S_{7/2}$ ground term of gadolinium where the orbital angular contribution is zero.

From the M vs. H curves, Fig. 5, the value of the magnetization at the higher magnetic field, 5 T, is 5.2 μ_B; this is smaller than the theoretical value expected for the Gd^{3+} ion: $\mu(Gd^{3+}) = gJ = 7\,\mu_B$. A ferrimagnetic ordering between Ir^{4+} and Gd^{3+} sublattices seems to be present that will justify this moment. This will be in agreement with the saturation moment expected for a two collinear sublattices model with ordered magnetic moments of 7 μ_B for Gd^{3+} and something higher than 1 μ_B for Ir^{4+} (due to a spin orbital contribution); the coupling between those two sublattices will result in an overall ferrimagnetic order, with a calculated moment of $\sim$5.8 μ_B that agrees rather well with the value of 5.2 μ_B obtained at saturation for this compound.

3.3. Structural details

3.3.1. The copper pyramid

From the distances presented on Table 2 one can see that copper sits in a square planar pyramid; from the Cu–O(2)–Cu angle, of 174.8°, we infer a buckling angle of 2.6°. This is indeed almost planar, close to what is observed in the mercury cuprates. Interestingly, this differs substantialy from the Ru and Cr cuprates where this angle was 168.7° [15,31] and 166.3° [15,22], respectively.

As for the copper–oxygen distances, the equatorial ones, 1.93 Å, are comparable to what is observed in this type of cuprates (c.f. 1.913 Å for $CrSr_2TRCu_2O_8$, 1.92 Å for $RuSr_2TRCu_2O_8$ and 1.91 Å for Ybco.) This shows that the copper–oxygen plane is quite stiff in the bonding distances and rather flexible in the bonding angles, an interesting situation.

On the other hand, the apical distance 2.30 Å is similar to that observed in Ybco (see Fig. 3 in Ref. [22]). The pyramid is then an elongated one, $r_{a/e} = 2.30/1.93 = 1.19$ (c.f 1.20 in Ybco)

3.3.2. The Ir–O polyhedron

It is also interesting to note that the [Ir–O_6] octahedron is a rather flattened one: the apical-to-equatorial ratio being $r_{a/e} = 1.81/1.99 = 0.93$. The [$Cr^{IV}$–$O_6$] octahedra were less flattened, $r_{a/e} = 0.97$, while the [Ru–O_6] octahedra in the rutheno-cuprate was almost regular, $r_{a/e} \approx 1$. As is the case of Cr^{IV}—a d^2 ion—Ir^{IV} (d^5) is a Janh–Teller ion. One is then tempted to attribute this flattening of the octahedra to a Janh–Teller effect on the t_{2g} electronic configuration. Yet, in this lower orbitals the Jahn–Teller effect is usually very small, even non-existing [33,40]. It is interesting to mention that when [Ir^{4+}–O_6] octahedra are located in Sr_2IrO_4, with the K_2NiF_4-type structure, obtained at room pressure, the octahedra is elongated, $r_{a/e} = 1.04$ (see Ref. [41]) which is opposite to what is seen here. Yet, we have to recall that, our material has been obtained at high pressure.

The octahedra are rotated ~14.8° around the *c*-axis which is comparable to the rhutenate and chromate. There is also a tilt of the octahedra away from the *c*-axis that can be obtained from the Ir–O–Cu angle, 165.2°, higher than in the chromate, 168.6°, and much higher than in the ruthenate, 173.2° when the tilt angle is the smallest. Due to the splitting of the O(1) position, this octahedral tilt is randomly distributed around the four possible positions shown on Fig. 2. This may have some consequences in the microstructure, see below.

3.4. Microstructure

Electron microscopy and diffraction, however, gave a more detailed view of the structure. The electron diffraction pattern in Fig. 6 shows a series of strong spots that can be indexed on the basis of the $[001]_p$ axis of a simple perovskite cell. This is the substructure common to these types of materials. Besides, one can also observe some, somewhat weaker, spots indexed as $h/2\,k/2\,0$, which suggest the presence of a so-called diagonal cell $a_p\sqrt{2} \times a_p\sqrt{2} \times na_p$; this is characteristic of many perovskite structures [42] or superstructures [31,43,44] when there is an octahedral tilt. If the tilt is regularly ordered within the crystal, the corresponding maxima can be observed in X-ray or neutron diffraction; however, if this tilt is not long-range ordered one can only see the diagonal cell by means of electron diffraction. Moreover, when the perovskite axial ratio is close to the ideal value of 3, microdomains are formed in which the long superstructure axis, in this case $3a_p$, is randomly distributed in one of the three space directions. This seems to be what happens in here, Fig. 6, in observing the spots present at $h/3\,0\,0$ and $0\,k/3\,0$ that treble the a^* and b^* perovskite axis. The whole

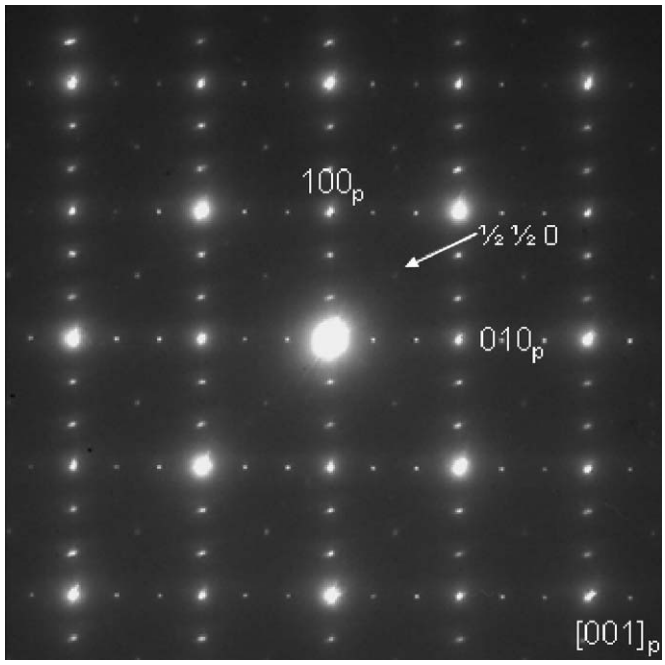

Fig. 6. Electron diffraction pattern of $IrSr_2GdCu_2O_8$ along the perovskite $[001]_p$ zone axis. Two threefold superstructures are present. Also there are spots at $h/2\,k/1\,0$ (h and k odd). See text for details.

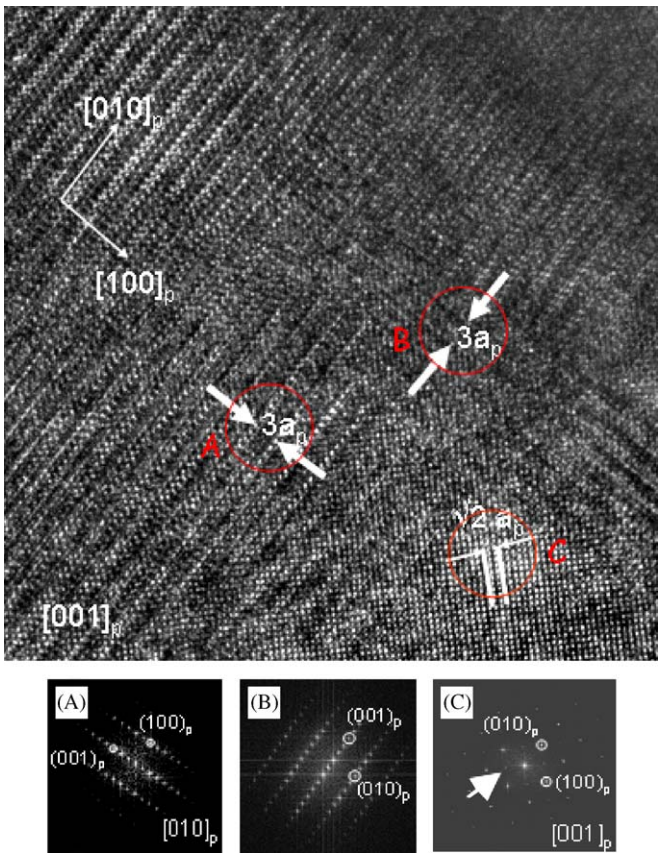

Fig. 7. A high-resolution electron micrograph showing a three-dimensional microdomain texture. The long *c*-axis of the supercell ($c = 3a_p \approx 11.5$ Å) is randomly distributed in the three space orientations: (a) Fourier transform of domain A, (b) Fourier transform of domain B and (c) Fourier transform of domain C.

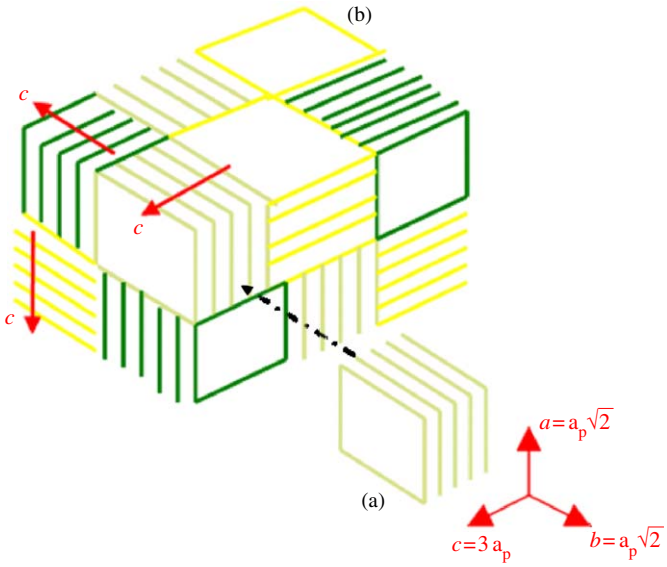

Fig. 8. Schematic, somewhat idealised, microdomain texture of $IrSr_2GdCu_2O_8$: (a) single domain and (b) multi-domain crystal.

situation is clearly confirmed by the corresponding electron micrograph appearing in Fig. 7a. Microdomains are observed in which the long c-axis ($d \approx 11.5$ Å) alternates at random in different regions of the crystal, along the three space directions.

Moreover, the Fourier transform of each of the different regions gives the corresponding pattern: zone axis $[110]_s \langle\rangle [010]_p$ (Fig. 7b), $[\bar{1}10]_s \langle\rangle [100]_p$ (Fig. 7c) and $[001]_s \langle\rangle [001]_p$ (Fig. 7d) where subindex s refers to the $a_p\sqrt{2} \times a_p\sqrt{2} \times 3a$ superstructure and subindex p refers to the basic perovskite cell ($a_p \approx 3.8$ Å); on the other hand, a combination of the three Fourier transforms gives, obviously, a pattern similar to the electron diffraction pattern in Fig. 6. A schematic representation of the microdomain situation is shown in Fig. 8. Fig. 8a shows a single domain and Fig. 8b shows the multi-domain crystal.

4. Conclusions

A new irido-cuprate material has been prepared at high pressure and high temperature. It shows the Ybco structure with the square planar [Cu–O_4] replaced by [Ir–O_6] octahedra. Ir appears to be tetravalent while copper is mixed valent: $Cu^{2.5+}$. The octahedra are substantially tilted with respect to the regular perovskite structure and this seems to be related to the very interesting three-dimensional microdomain texture observed.

A ferrimagnetic ordering of the Ir and Gd sublattices is present. This seems to be the first example of ferrimagnetism in the M-1212 family of cuprates.

Neutron diffraction experiments, using the ^{160}Gd isotope, are planned to confirm this model and establish the magnetic structure of this very interesting mixed oxide.

Acknowledgments

We acknowledge financial support from CICYT, program MAT 2004-01641 and Fundación Areces (Ayudas 2002). We also thank Dr. J.M. Gallardo Amores for technical assistance.

References

[1] L. Bauernfein, W. Widder, H.D. Braun, Physica C 254 (1995) 151.
[2] I. Felner, U. Asaf, S. Reich, T. Tasabba, Physica C 311 (1999) 163.
[3] L. Bauernfein, W. Widder, H.D. Braun, J. Low Temp. Phys. 105 (1996) 1605.
[4] I. Felner, U. Asaf, F. Ritter, P.W. Klamut, B. Dabrowski, Physica C 368 (2001) 364–365.
[5] A. McLaughlin, J.P. Attfield, Phys. Rev. B: Solid State 60 (1995) 14605.
[6] Y. Tokura, H. Takagi, S. Uchida, Nature 337 (1989) 345.
[7] M.Á. Alario-Franco, Adv. Mater. 7 (2) (1994) 229.
[8] C. Greaves, P.R. Slater, Physica C 161 (1989) 245.
[9] N. Murayama, E. Sudo, K. Kani, A. Tsuzuki, S. Kawakami, M. Awano, Y. Torii, Jpn. J. Phys. 27 (9, Part 2) (1998) 9.
[10] T. Kawashima, E. Takayama-Muromachy, J. Magn. Magn. Mater. 227–276 (2004) e167–e168.
[11] A. Butera, A. Fainstein, E. Winkler, J. Tallon, Phys. Rev. B. 63 (2001) 054442.
[12] V.L. Ginzburg, Zh. Exsp. Teor. Fiz. 31 (1956) 202.
[13] L. Bernd, C. Ching-Wu, Nat. Mater. 4 (7) (2005) 516–517.
[14] M. Fauré, A.I. Buzdin, Phys. Rev. Lett. 94 (2005) 187202.
[15] R. Ruiz-Bustos, Ph.D. Thesis, Universidad Complutense, Madrid, Spain, 2003.
[16] R. Ruiz-Bustos, J.M. Gallardo-Amores, R. Sáez-Puche, E. Morán, M.Á. Alario-Franco, Physica C 382 (2002) 395.
[17] R. Ruiz-Bustos, M.H. Aguirre, E. Morán, R. Sáez-Puche, M.Á. Alario-Franco, Curr. Appl. Phys. 2 (2002) 461.
[18] A.C. Mclaughlin, J.P. Attfield, Phys. Rev. B. 60 (1999) 14605.
[19] P.W. Klamut, B. Dabrowski, S. Kolesnik, M. Maxwell, J. Mais, Phys. Rev. B. 63 (2001) 224512.
[20] S. Andrade, F.C. Fonseca, R.F. Jardim, I. Bossi, M.S. Torikachvili, A.H. Lacerda, L. Ben-Dor, Braz. J. Phys. 33 (4) (2003).
[21] M.S. Torikachvili, I. Bossi, J.R. O'Brien, F.C. Fonseca, R. Muccillo, R.F. Jardim, Physica C 408–410 (2004) 195–196.
[22] R. Ruiz-Bustos, M.H. Aguirre, M.Á. Alario-Franco, Inorg. Chem. 44 (2005) 3063–3069.
[23] R. Ruiz-Bustos, J.M. Gallardo-Amores, E. Morán, J.P. Attfield, R. Sáez-Puche, M.Á. Alario-Franco, Mater. Res. Soc. Symp. 659 (2001) II11.6.1.
[24] R. Ruiz-Bustos, J.M. Gallardo-Amores, E. Morán, M.Á. Alario-Franco, High Pressure Res. 22 (2002) 573–576.
[25] Y. Tokunaga, H. Kotegawa, K. Ishida, Y. Kitaoka, H. Takagiwa, J. Akimitsu, Phys. Rev. Lett. 86 (2001) 5767.
[26] J. Rodríguez-Carvajal, FULLPROF: A program for Rietveld refinement and pattern matching analysis, in: The Abstract of the Satellite Meeting of the XVth Congress of the International Union of Crystallography, Toulouse, France, (Université Paul Sabatier, Toulouse), 1990, p. 127.
[27] A. Niazi, P.L. Paulose, E.V. SampathKumaran, Phys. Rev. Lett. 88 (10) (2002).
[28] A. Niazi, P.L. Paulose, E.V. SampathKumaran, Ute C.H. Rodewald, W. Jeitschko, J. Phys. 58 (5 & 6) (2002).
[29] M. Takano, Y. Takeda, H. Okada, M. Miyamoto, T. Kusaka, Physica C: Superconductivity 159 (1989) 375.
[30] R. S Liu, L.Y. Jang, H.H. Hung, J.L. Tallon, Phys. Rev. B 63 (2001) 212507.
[31] A.C. McLaughlin, W. Zhow, J.P. Attfield, A.N. Fitch, J.L. Tallon, Phys Rev. B: Solid State 60 (1999) 7512.
[32] K. Hayashi, G. Demazeau, M. Pouchard, P. Hagenmuller, MRB 15 (1980) 461–467.
[33] F.A. Cotton, G. Wilkinson, P.L. Gauss, Basic Inorganic Chemistry, Wiley, New York, 1995.
[34] J. Darriet, G. Demazeau, M. Pouchard, MRB 16 (1981) 1013–1017.
[35] M. Kotani, J. Phys. Soc. Jpn. 4 (1949) 293.
[36] E.M. Ramos, I. Alvarez, R. Sáez-Puche, M.L. Veiga, C. Pico, J. Alloy. Compd. 225 (1995) 212–215.
[37] F.E. Mabbs, D.J. Machin, Magnetism and Transition Metal Complexes, William Clowes and Sons, London, 1973, p. 21.
[38] E.V. Antipov, A.M. Abukamov, S.N. Putilin, Supercond. Sci. Technol. 15 (2002) R31–R49.
[39] R.L. Carlin, Magneto-chemistry, Springer, Berlin, Heidelberg, New York, Tokyo, 1986, p. 142.
[40] N. Greenwood, A. Earnshaw, Chemistry of the Elements, Pergamon Press, Elmsford, NY, 1984.
[41] T. Shimura, Y. Inaguma, T. Nakamura, M. Itoh, Phys. Rev. B, V 52 (13) (1995) 9143–9146.
[42] A. Vegas, M. Vallet-Regí, J. Gonzalez-Calbet, M.Á. Alario-Franco, Acta Cryst. B 42 (1986) 167.
[43] M. Aguirre, R. Ruiz-Bustos, M.Á. Alario-Franco, J. Mater. Chem. 13 (5) (2003) 1156–1160.
[44] R.H. Mitchell, Perovskites: Modern and Ancient, Almaz Press, Ont., Canada, 2002.